

AD-A058 483

REGIS COLL WESTON MASS  
AN INITIAL STUDY OF POWER SPECTRA FROM SATELLITE IMAGERY, (U)

F/G 4/2

SEP 78 R F FOURNIER

F19628-77-C-0010

UNCLASSIFIED

SCIENTIFIC-2

AFGL-TR-77-0295

NL

1 OF 1

AD  
A058 483



A microfiche card containing 35 frames of data. The frames are arranged in a grid:

- Row 1: 13 frames. Frame 13 is a satellite image of a coastal region.
- Row 2: 13 frames. Frame 1 is a satellite image of a coastal region.
- Row 3: 8 frames. Frame 8 is a table of data.

END  
DATE  
FILMED  
11-78

DDC

ADA 058483

AFGL-TR-77-0295

LEVEL II

12  
B.S.

AN INITIAL STUDY OF POWER SPECTRA  
FROM SATELLITE IMAGERY

Ronald F. Fournier

Regis College  
235 Wellesley Street  
Weston, Massachusetts 02193

AD No. ~~1~~  
DDG FILE COPY

30 September 1978

Scientific Report No. 2

DDC  
SEP 12 1978  
97 F

Approved for public release; distribution unlimited

AIR FORCE GEOPHYSICS LABORATORY  
AIR FORCE SYSTEMS COMMAND  
UNITED STATES AIR FORCE  
HANSCOM AFB, MASSACHUSETTS 01731

78 08 16 073

Qualified requestors may obtain additional copies from the Defense Documentation Center. All others should apply to the National Technical Information Service.



Unclassified

SECURITY CLASSIFICATION OF THIS PAGE (When Data Entered)

REPORT DOCUMENTATION PAGE		READ INSTRUCTIONS BEFORE COMPLETING FORM	
1. REPORT NUMBER AFGL-TR-77-0295	2. GOVT ACCESSION NO.	3. RECIPIENT'S CATALOG NUMBER	
4. TITLE (and Subtitle) AN INITIAL STUDY OF POWER SPECTRA FROM SATELLITE IMAGERY		5. TYPE OF REPORT & PERIOD COVERED Scientific Report Number 2 Period ending 30 September 77	
7. AUTHOR(s) Ronald F. Fournier		8. CONTRACT OR GRANT NUMBER(s) F19628-77-C-0010	
9. PERFORMING ORGANIZATION NAME AND ADDRESS Regis College 235 Wellesley Street Weston, Massachusetts 02193		10. PROGRAM ELEMENT, PROJECT, TASK AREA & WORK UNIT NUMBERS 61102F 2310G2AF	
11. CONTROLLING OFFICE NAME AND ADDRESS Air Force Geophysics Laboratory Hanscom AFB, Massachusetts 01731 Contract Monitor: Peter A. Giorgio, LY		12. REPORT DATE 30 September 1978	
14. MONITORING AGENCY NAME & ADDRESS (if different from Controlling Office)		13. NUMBER OF PAGES 34	
		15. SECURITY CLASS. (of this report) Unclassified	
		15a. DECLASSIFICATION/DOWNGRADING SCHEDULE	
16. DISTRIBUTION STATEMENT (of this Report) Approved for public release; distribution unlimited  (12) 35 p.			
17. DISTRIBUTION STATEMENT (of the abstract entered in Block 20, if different from Report)  (14) Scientific-2			
18. SUPPLEMENTARY NOTES			
19. KEY WORDS (Continue on reverse side if necessary and identify by block number) pixel 3-D Nephanalysis Sikula Nyquist			
20. ABSTRACT (Continue on reverse side if necessary and identify by block number) Air Force Global Weather Center (AFGWC) routinely generates a global cloud analysis called 3-D Nephanalysis (3-D Neph). At 15 levels in the atmosphere and for 25-mile square boxes, the cloud field is defined as clearly as possible with available data. All modes of data (surface, radiosonde, aircraft and satellite), are pre-processed and used prior to utilization by 3-D Neph by means of a decision tree process. This report reviews briefly the current approach at AFGWC, and the proposed method of processing increased amounts of data with a higher level of sophistication and greater efficiency.			

DD FORM 1 JAN 73 1473

EDITION OF 1 NOV 65 IS OBSOLETE

Unclassified

SECURITY CLASSIFICATION OF THIS PAGE (When Data Entered)

302.000



SECURITY CLASSIFICATION OF THIS PAGE(When Data Entered)

[The main body of the page is a large, empty rectangular box with a black border, intended for the entry of security classification data.]

SECURITY CLASSIFICATION OF THIS PAGE(When Data Entered)

TABLE OF CONTENTS

	Page
1. Introduction . . . . .	1
2. Approach . . . . .	3
2.1 Nature of the Problem . . . . .	3
2.2 The 3-D Nephanalysis Concept. . . . .	8
2.3 Scope of Investigation. . . . .	8
3. The Satellite Processor. . . . .	9
4. The Fast Fourier Transform (FFT) . . . . .	12
5. Normalized Averaged Power Spectra Computation. . . . .	14
6. A Study of Two Cloud Areas . . . . .	19
7. Conclusion . . . . .	25
8. Future Work. . . . .	26

ACCESSION for	
NTIS	White Section <input checked="" type="checkbox"/>
DDC	Buff Section <input type="checkbox"/>
UNANNOUNCED JUSTIFICATION	<input type="checkbox"/>
BY	
DISTRIBUTION/AVAILABILITY CODES	
or SPECIAL	
A	

78 08 16 073

LIST OF ILLUSTRATIONS

	Page
1. McIDAS display of block 5C DMSP data resolved at (a) 3 nm, and (b) 1/3 nm . . . . .	4-7
2. (a) Background brightness range factors as a function of background brightness; (b) Adjusted average bright- ness versus percent cloudiness for ESSA-9 . . . . .	10
3. Schematic of Fast Fourier Transform (FFT) output power terms of quadrant I duplicated in quadrants II, III and IV. Each two digit group represents a two dimensional FFT coefficient of power $P_{j,i}$ where $j$ represents the first digit and $i$ represents the second digit of a 25 x 25 nm box . . . . .	16
4. Schematic of the annular bands that are integrated in computing normalized averaged amplitudes (NAA) from Fast Fourier Transform coefficients ( $P_{j,i}$ ) for the six frequencies of a 25 x 25 nm box . . . . .	17
5. Mean normalized averaged amplitudes (NAA) for 64 - 25 x 25 nm boxes as a function of frequency for area 1. . . . .	20
6. Mean normalized averaged amplitudes (NAA) for 64 - 25 x 25 nm boxes as a function of frequency for area 2. . . . .	20
7. Normalized averaged amplitudes (NAA) for the 200 x 200 nm box as a function of frequency for area 1 . . . . .	21
8. Normalized averaged amplitudes (NAA) for the 200 x 200 nm box as a function of frequency for area 2 . . . . .	21
9. Variance of normalized averaged amplitudes (NAA) for 64 25 x 25 nm boxes as a function of frequency for area 1 . . . . .	23
10. Variance of normalized averaged amplitudes (NAA) for 64 25 x 25 nm boxes as a function of frequency for area 2 . . . . .	23



LIST OF TABLES

	Page
1. The statistic T' for comparison of differences in mean normalized averaged amplitudes (NAA) for area 1 and area 2 . . . . .	27
2. The statistic F in comparison with variance in normalized averaged amplitudes (NAA) for area 1 and area 2 . . . . .	28

## 1.0 Introduction

There are two claims about meteorological satellites which are not likely to be challenged. The first claim is that they have provided us with an abundance of data, and the second is that the data have not been converted into information in a very efficient manner. The reasons for this inefficiency are:

1. Hard-copy imagery, although a valuable tool in the hands of a skilled analyst, suffers from inconsistency in interpretation, is expensive to distribute widely, and is time-consuming to process in the variety of formats the analyst might need.

2. Techniques and the hardware to process data objectively are inadequate to handle the overwhelming volume of data transmitted by both polar orbiting and geosynchronous satellites.

The difficulties with hard-copy imagery are, to a large extent, being overcome with interactive systems such as McIDAS (Man-computer Interactive Data Access System) which combine the speed of electronic image processing with the judgement of the skilled analyst.

Objective processing, on a rudimentary level, has been taking place at the Air Force Global Weather Central (AFGWC) since 1971 (Coburn 1971) to support the specification and forecasting of global cloud cover. Satellite data are combined with surface, radiosonde and aircraft observations to produce a 15-level global cloud distribution with a horizontal resolution of 25 miles square. This product, named 3-D Nephanalysis, is used, among other ways, as the initial condition for the cloud forecast in the global numerical forecast. The AFGWC is the only operational group that attempts to exploit satellite imagery in an automated process.

Despite AFGWC's leadership in the application of satellite data, requirements placed on them by their customers exceed their processing capability. Presently, smoothed mode data at approximately 3 nm resolution are used as the satellite input to the 3-D Nephanalysis although fine mode data at 1/3 nm resolution are sensed by the satellite. The fine mode data are displayed as hard copy but are not otherwise used because until recently the AFGWC computers were completely inadequate to operate in real time with the rates and volume of data involved.

This report discusses some initial efforts the Regis College Research Center directed toward the development of methods of improving the 3-D Nephanalysis by the use of fine mode data and eventually the development of a model that uses only satellite data to define the cloud cover.



## 2.0 Approach

### 2.1 The Nature of the Problem

Improvement of operational cloud specification at AFGWC by means of the utilization of fine mode data poses two problems. The first problem is how to handle the enormous quantities of data involved. The fine mode sensor of the Block 5-D system generates over 100 times as much data as the high resolution sensor in the Block 5-C system.

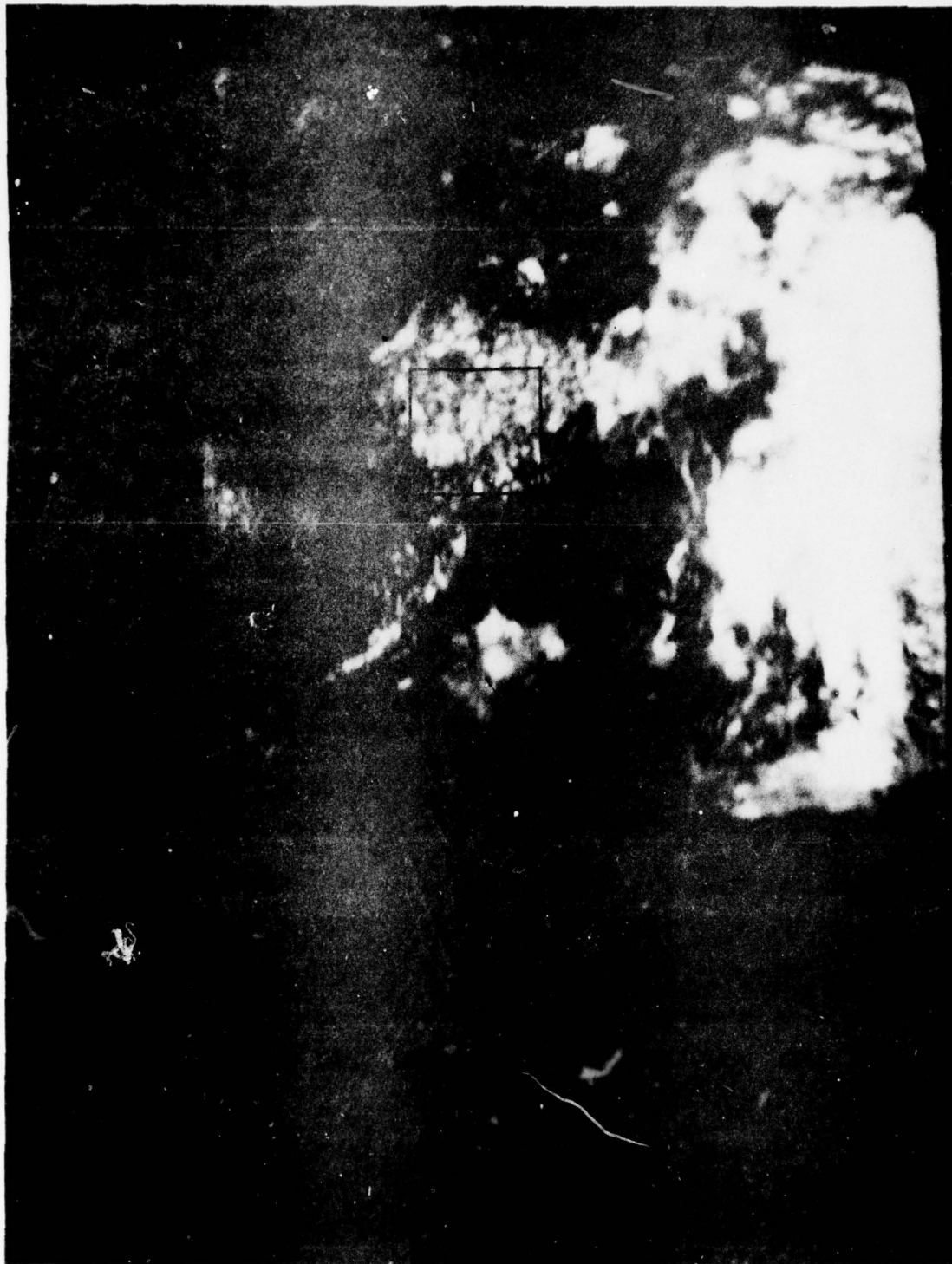
Figure 1 illustrates what this 100-fold increase in data means in terms of the amount and quality of the data. The images, photographed on the McIDAS screen, are Block 5-C, fine mode data processed so as to simulate Block 5-D smoothed mode (3 nm) data in Fig. 1a and fine mode (1/3 nm) data in Fig. 1b. Each of these displays contain 149,500 6-bit picture elements. The ratio of the area covered by these 2 million bits of fine mode data is illustrated by the size of the outlined box to the entire display in Fig. 1a.

The second problem of providing improved information content using significantly larger amounts of data can be approached by developing:

- a. better software
- b. better/more hardware
- c. a combination of improved software and hardware

Considering the magnitude of the data involved, sophisticated programming alone could not come close to alleviating the problem. More and larger computers are an expensive way to go. The approach selected by AFGWC and AFGL was to utilize sophisticated analytical techniques which are adaptable to hard wired computational devices. Specifically, this report discusses preliminary attempts to utilize coefficients of Fast Fourier Transforms (FFT) as indices of cloud types. Although any success in this approach may not be

Fig. 1a Block 5-C fine mode (1/3 nm) data processed so as to simulate Block 5-D smoothed mode (3 nm) data. The outlined area is over Central America. The photograph was taken from the AGFL McIDAS display.





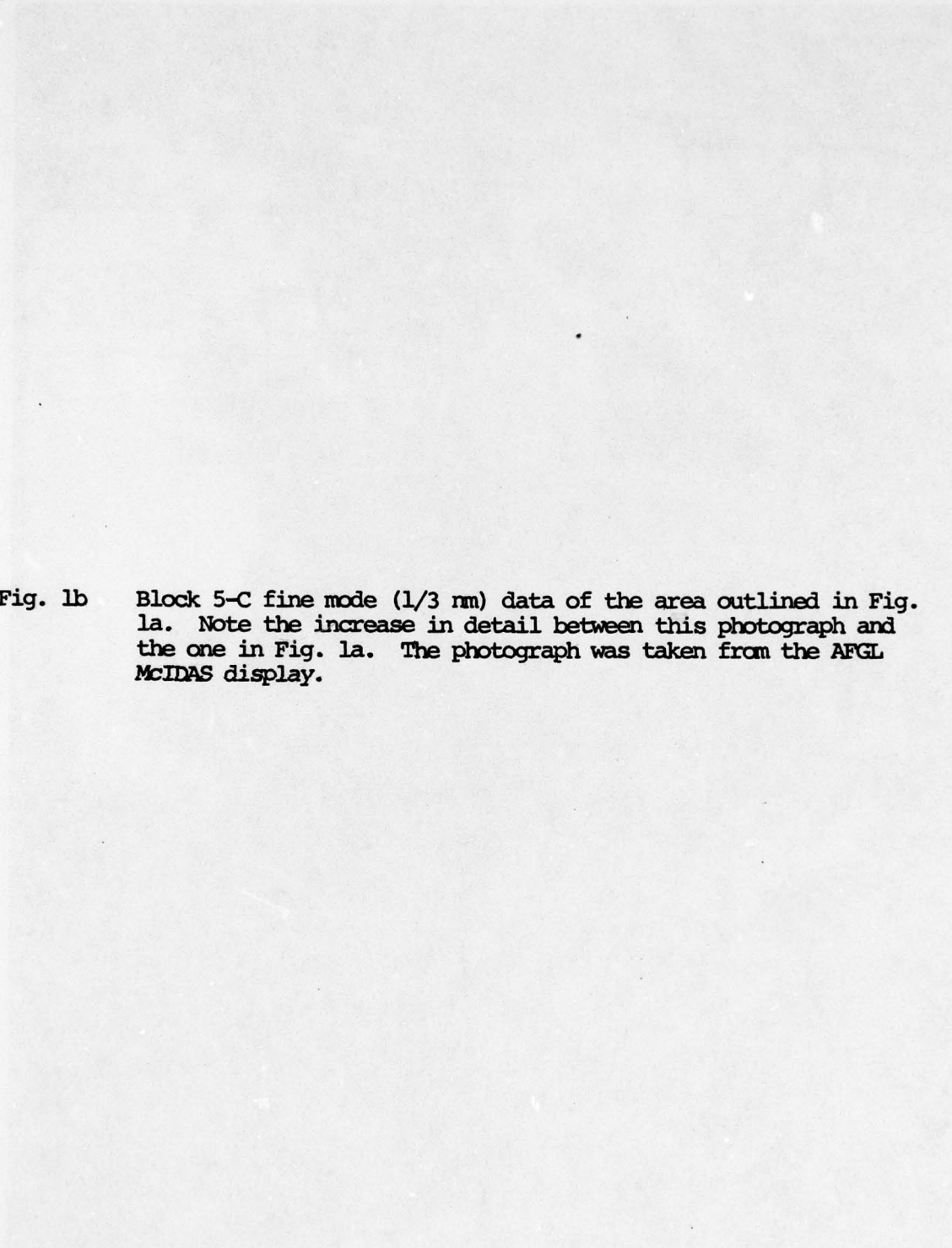


Fig. 1b Block 5-C fine mode (1/3 nm) data of the area outlined in Fig. 1a. Note the increase in detail between this photograph and the one in Fig. 1a. The photograph was taken from the AFGL McIDAS display.



immediately applicable to AFGWC operations, it could influence a decision to invest in "black boxes" to perform the enormous amount of "number crunching" involved in real-time FFT computations.

## 2.2 The 3-D Nephanalysis Concept

In the 3-D Nephanalysis model now being used, cloud characteristics are defined in boxes approximately 25 miles square over the earth. All available data - satellite, surface, radiosonde and aircraft - are used as input. The output, insofar as the input allows, specifies the amount of cloudiness at 15 levels in the atmosphere; the type of cloud identified as cumulus, stratus, cumulonimbus, etc; cloud base and top; and type of precipitation. Over remote areas where only satellite data are available, only the amount, type, and tops of the clouds can be specified. When contradicting observations, such as a difference in the cloud amount reported by a ground observer and the satellite algorithm, are received, the model makes a decision based on a data-reliability decision tree.

## 2.3 Scope of Investigation

This investigation is concerned with just that part of the 3-D Nephanalysis that treats satellite data. It is called the satellite processor and is the software that converts the satellite-observed brightness and/or temperature into cloud categories. In this report we will be dealing only with Block 5-C visual data because of some unanticipated delays in the availability of Block 5-D data.



### 3.0 The Satellite Processor

The satellite processor stage of the 3-D Nephanalysis currently documented by AFGWC<sup>1,2</sup> uses both visual and infrared data. The visual data, which we are using exclusively at this time, generate two cloud-identification indices. The first index, V, is the average deviation of the 64 brightness values in each 25 mi. sq. box. The second index, A, is an adjusted average brightness:

$$A = (\bar{B} - M7)F_B ,$$

where:

$\bar{B}$  is the average brightness of a 25 x 25 mi box,

M7 is a seven-day average of background brightness,

$F_B$  is an empirically derived background brightness range factor.

Figure 2a is a graph of  $F_B$  as a function of background brightness. Figure 2b is a graph of the adjusted average brightness (A) incorporating the background brightness range factors ( $F_B$ ) versus cloud cover for the ESSA-9 satellite.<sup>1</sup>

In the visual data processor the type of cloud is determined from the adjusted average brightness (A) and the average deviation (V), using the following set of conditions:

- 1) If  $V = 3$ , broken cloud conditions or variable cloud tops with the type defined as Cumulus.
- 2) If  $V \leq 3$  and  $A \geq 56$ , the type of cloud is defined as Cumulonimbus.

- 
1. Maj. Coburn, A.R., "Improved Three Dimensional Nephanalysis Model", AFGWC Technical Memorandum 71-2, 1 June 1971.
  2. Capt. Fye, F.K., and Capt. G.L. Logan, "AFGWC Satellite Based Analysis and Prediction Programs", Proc. 7th Technical Eacl. Conference, Atmosphere Sciences Lab, White Sands Missile Range, NM April 1977.

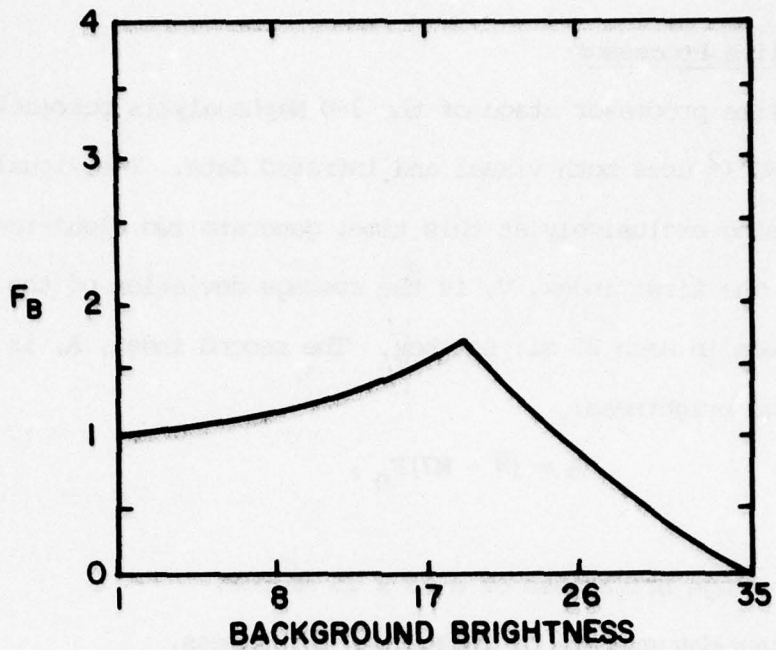


FIG. 2A BACKGROUND BRIGHTNESS RANGE FACTORS ( $F_B$ ) AS A FUNCTION OF BACKGROUND BRIGHTNESS.

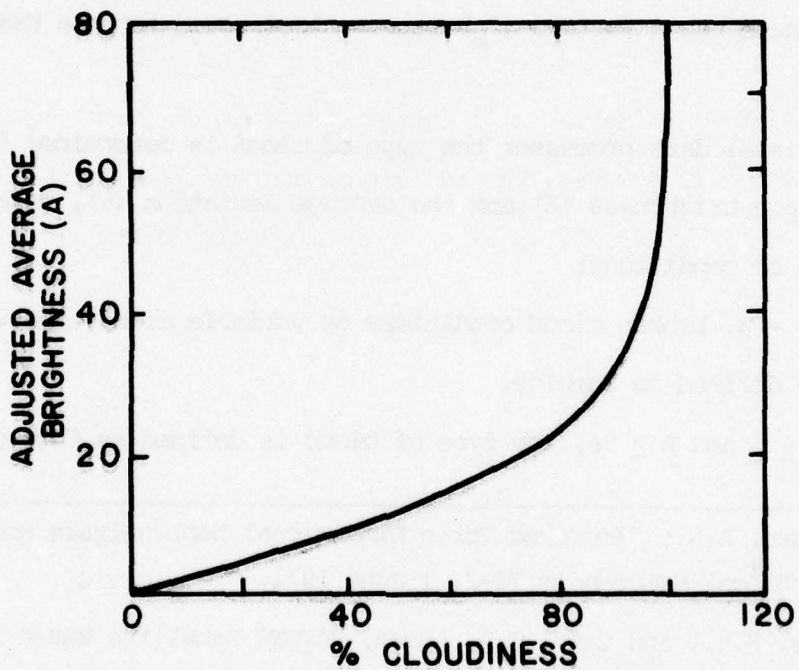


FIG. 2B ADJUSTED AVERAGE BRIGHTNESS VS PERCENT CLOUDINESS FOR ESSA 9.

3) If  $V > 3$  and  $A < 56$ , the type of cloud is defined as Stratus.

Infrared data are not classified into cloud types but are used to provide cloud-top height input for the 3-D Nephanalysis. Information that is given by both the visual and infrared data processors are put into a data base for subsequent use by 3-D Nephanalysis.

It is possible to obtain the same information using FFT output processing. With the present data flow structures at AFGWC, incorporation of FFT output processing will not require major data flow alterations. From a software standpoint, incorporation of FFT output processing can be achieved by adding a subroutine to the present satellite processor. Depending upon the manner in which the FFT output is processed, it is possible to extract from the imagery even more information than the current visual and infrared processors give. As demonstrated by Booth<sup>3</sup>, FFT output processing of dual channel (IR and visual) imagery can yield cloud classification for a larger number of cloud types than is now available at AFGWC. Operating on the FFT output in a different fashion will extract information about the alignment of cloud bands. If, however, the additional information is to be incorporated, many data flow structures within 3-D Nephanalysis and the satellite processor will require modification.

---

3. Booth, A.L., "Cloud Type Pattern Recognition Using Environmental Satellite Data", First International Joint Conference on Pattern Recognition, 30 October - 1 November 1973.



#### 4.0 The Fast Fourier Transform (FFT)

The Fourier Transform in the past has been utilized for characterizing linear systems and for identifying the frequency components making up a continuous waveform. However, when the waveform is sampled, or the system is to be analyzed on a digital computer, it is the finite, discrete version of the Fourier Transform that must be used. The Fast Fourier Transform (FFT), as developed by Cooley and Tukey, is simply an efficient method for computing the discrete Fourier Transform.

The Fourier Transform for a continuous waveform can be written as:

$$1a) \quad Y(f) = \int_{-\infty}^{\infty} X(t) \exp(-2\pi i f t) dt$$

$$1b) \quad X(t) = \int_{-\infty}^{\infty} Y(f) \exp(+2\pi i f t) df$$

where

$Y(f)$  is the frequency domain function,

$X(t)$  is the time domain function,

$$i = \sqrt{-1}$$

The analogous discrete Fourier Transform pair can be written as:

$$2a) \quad Y(j) = \frac{1}{N} \sum_{k=0}^{N-1} X(k) \exp(-2\pi j k i / N)$$

$$2b) \quad X(k) = \sum_{j=0}^{N-1} Y(j) \exp(+2\pi j k i / N)$$

where,  $Y(j)$  is analogous to  $Y(f)$  in 1a,  $X(k)$  is analogous to  $X(t)$  in 1b, and  $N$  is the number of points sampled. The discrete Fourier Transform can be computed from equations 2a and 2b directly, but it is slower than using the FFT. For an  $N$  point transformation, where  $N=2^m$  ( $m$  is a positive integer), the number of complex additions and subtractions is given by  $N^2$ . For the FFT the number of complex additions and subtractions is reduced to

$(N/2) \log_2 N$ . For  $N = 1024$  this represents a savings of over 200 to 1.

The output of an FFT is simply the coefficients of a Fourier series representation of a function. A one-dimensional Fourier series representation of a function reduces to a simple harmonic expressed by:

$$3) F(x) = A_0 + \sum_{j=1}^{\infty} (A_j \cos(\frac{2n\pi x}{T}) + B_j \sin(\frac{2n\pi x}{T}))$$

where,

T = period of the function

x = sampled domain

j = phase

and  $A_0$ ,  $A_j$ , and  $B_j$  are the coefficients. For a one-dimensional FFT of an 8-pixel scan line the output consists of the 17 coefficients  $A_0$ ,  $A_j$ , and  $B_j$ , with j ranging from 1 to 8. In a two-dimensional FFT of an 8 x 8 pixel area the output would consist of the 129 coefficients  $A_{0,0}$ ,  $A_{j,i}$ , and  $B_{j,i}$  with j and i ranging from 1 to 8. The two-dimensional FFT coefficients are then used to compute the power spectrum. The proper processing of spectra will extract information from the imagery field.

## 5.0 Normalized Average Power Spectra Computation

When a power spectrum is computed from 2-dimensional Fourier Transform coefficients, a new set of parameters is generated in response to the spatial distribution and frequency characteristics of the data field. Both Sikula<sup>4</sup> and Booth<sup>2</sup> demonstrated that some cloud types generate reproducible power spectra parameters, i.e., identifiable spectral signatures. These spectral signatures indicate size, shape and texture of a particular cloud type. The power spectrum can be interpreted as the amount of variance in an imagery field due to clouds of various sizes. Booth<sup>2</sup> demonstrated that by proper utilization of power spectra one can classify clouds by using a discriminant function once the boundaries of the cloud classes were determined.

As an initial step, power spectra were computed by annularly integrating the FFT coefficients. It is advantageous to compute power spectra in annular rings since the FFT retains the property of a periodic function allowing duplication of FFT output as a half-range expansion. Figure 3 schematically illustrates this concept. Each two digit group seen in Figure 3 represents a two-dimensional FFT coefficient of power. Power is defined as

$$P_{j,i} = \sqrt{A_{j,i}^2 + B_{j,i}^2},$$

if  $A_{j,i}$  is the real part (Cosine term coefficient) and  $B_{j,i}$  is the imaginary part (Sine term coefficient). The  $j$  represents the first digit and  $i$  represents the second digit in each two digit group of Figure 3. The periodicity of the Fourier Transform allows duplication of the FFT output in quadrant I,

---

4. Capt. Sikula, G.J., "Spectral Signatures of Several Cloud Types and Information from Very High Resolution Visual Satellite Radiances - Preliminary Results", Sixth Conference of Aerospace and Aeronautical Meteorology, 12-14 November 1974.



into the II, III, IV quadrants of Figure 3.

There is a factor that must be considered in discrete Fourier Transform processing because it may bias the power spectra that has been annularly integrated. This factor is called aliasing. Aliasing is the result of high-frequency components impersonating low-frequency components. Aliasing is minimized by computing the last half of the FFT output by symmetric complex conjugates. The coefficients for frequencies higher than the linear foldover frequency (or linear Nyquist frequency equal to  $f_s/2$ , where  $f_s$  is the sampled domain) are computed by symmetric complex conjugates of frequencies lower than the linear Nyquist. Since the power spectrum is integrated on a two-dimensional plane from the output of a two-dimensional FFT, it is acceptable to integrate the spectra annularly up to what is termed the two-dimensional Nyquist frequency, given by:

$$\sqrt{\frac{(\text{sample size of first dimension})^2}{4} + \frac{(\text{sample size of second dimension})^2}{4}}$$

Thus for a box in which there are 8 x 8 picture elements (pixels) the two-dimensional Nyquist frequency is approximately 6. Treating each two digit number in Figure 3 as a (j,i) coordinate, a distance from 00 ( $P_{0,0}$ ) can then be computed. Then the terms ( $P_{j,i}$ ) with the same distance from  $P_{0,0}$  are summed. Power terms that are the same distance from  $P_{0,0}$  can be seen in the alternating gray and white bands of Figure 4. Power terms that are above the two-dimensional Nyquist (distance is greater than 6) are folded back over into lower bands by subtracting each digit from the order of the imagery array. That is why the power terms above  $P_{6,6}$  in Figure 4 are in a band of smaller distance from  $P_{0,0}$ . Integration of the FFT coefficients in each annular band using this technique is done by running through the FFT output

QUADRANT II								$j$	QUADRANT I							
70	71	72	73	74	75	76	77	70	71	72	73	74	75	76	77	
60	61	62	63	64	65	66	67	60	61	62	63	64	65	66	67	
50	51	52	53	54	55	56	57	50	51	52	53	54	55	56	57	
40	41	42	43	44	45	46	47	40	41	42	43	44	45	46	47	
30	31	32	33	34	35	36	37	30	31	32	33	34	35	36	37	
20	21	22	23	24	25	26	27	20	21	22	23	24	25	26	27	
10	11	12	13	14	15	16	17	10	11	12	13	14	15	16	17	
00	01	02	03	04	05	06	07	00	01	02	03	04	05	06	07	
70	71	72	73	74	75	76	77	70	71	72	73	74	75	76	77	
60	61	62	63	64	65	66	67	60	61	62	63	64	65	66	67	
50	51	52	53	54	55	56	57	50	51	52	53	54	55	56	57	
40	41	42	43	44	45	46	47	40	41	42	43	44	45	46	47	
30	31	32	33	34	35	36	37	30	31	32	33	34	35	36	37	
20	21	22	23	24	25	26	27	20	21	22	23	24	25	26	27	
10	11	12	13	14	15	16	17	10	11	12	13	14	15	16	17	
00	01	02	03	04	05	06	07	00	01	02	03	04	05	06	07	
QUADRANT III									QUADRANT IV							

Fig. 3 Schematic of Fast Fourier Transform (FFT) output power terms of quadrant I duplicated in quadrants II, III, and IV. Each two digit group represents a two-dimensional FFT coefficient of power  $P_{j,i}$  where  $j$  represents the first digit and  $i$  represents the second digit of a 25 x 25 nm box.

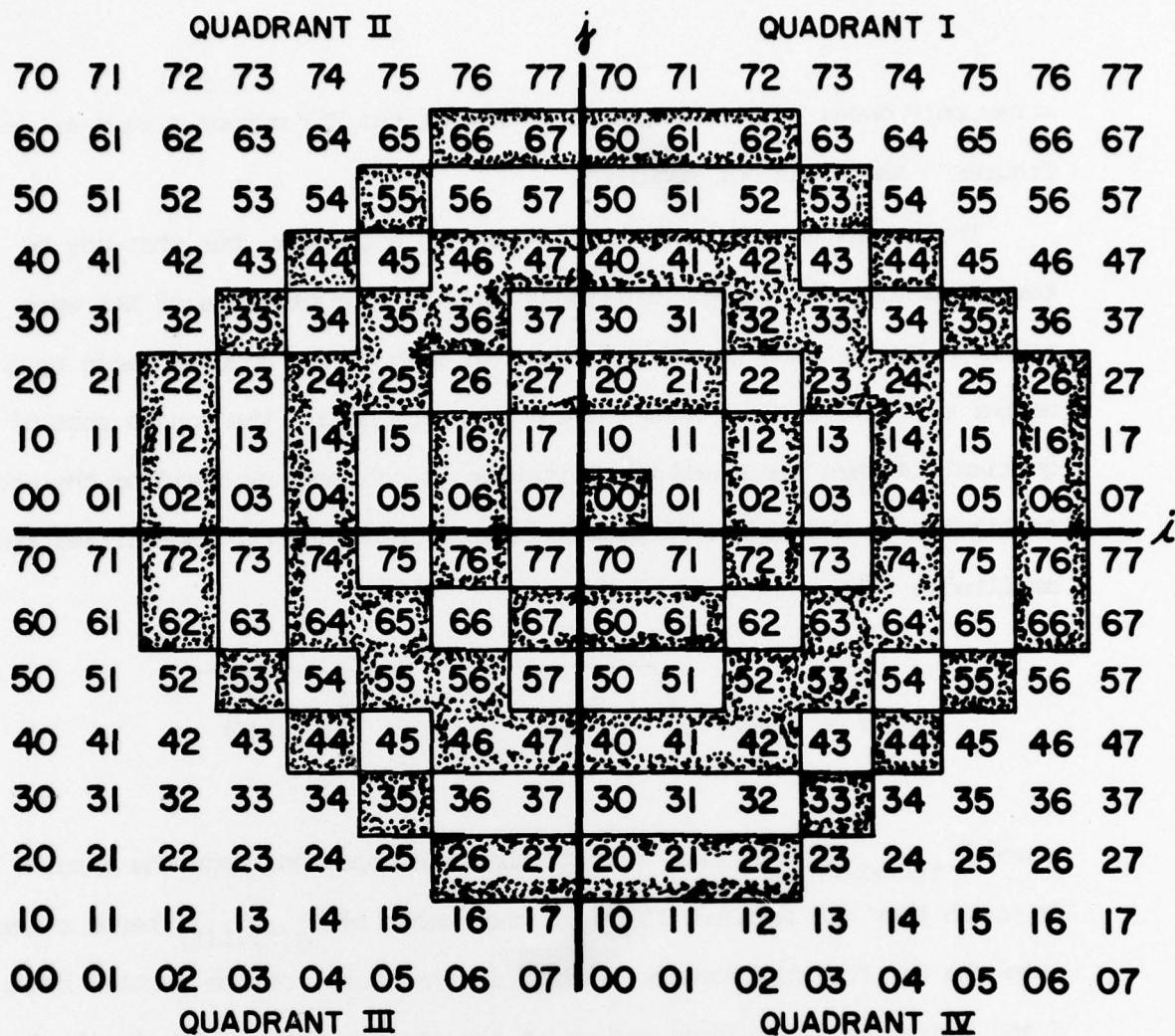


Fig. 4 Schematic of the annular bands that are integrated in computing normalized average amplitudes (NAA) from Fast Fourier Transform coefficients ( $P_{j,i}$ ) for the six frequencies of a 25 x 25 nm box.



array only once. Therefore, duplication of the FFT output arrays as seen in Figures 3 and 4 was not required.

The actual computation that is made is not power, but what may be termed normalized average amplitudes (NAA). Computations of NAA were achieved by dividing the summed power in each of the annular bands by the number of terms entered into the sum for each band. The square root of the quotient is then taken and normalization is achieved by dividing the average amplitudes by the number of pixels entered into the FFT. Normalized average amplitudes (NAA) can be expressed by:

$$NAA(f) = \frac{1}{J \cdot I} \sqrt{\frac{1}{NT(f)} \sum_{i=1}^I \sum_{j=1}^J P_{j(f),i(f)}^2}$$

where  $P_{j(f),i(f)}$  are power spectra that are dependent upon the annular band in which they are located;  $NT(f)$  is the number of  $P_{j(f),i(f)}$  terms entered into the sum for each annular band;  $f$  is the number of the annular band;  $J$  and  $I$  are the dimensional orders of the imagery array. For  $8 \times 8$  pixels where  $J = 8$  and  $I = 8$  normalization is achieved by dividing by the product of  $J \cdot I = 64$ . Each of the annular bands seen in Figure 4 has a unique number attached to it called the wave number or frequency. This unique number is actually the two-dimensional distance from the  $P_{0,0}$  term. In essence,  $P_{0,0}$  is the first band, consisting of only one term, and is said to be of frequency 0. The first white annular band, in Figure 4, consisting of eight terms, is frequency 1. The gray annular band following the frequency 1 white band consists of twelve terms and is frequency 2. This numbering scheme continues out to frequency 6, the outer gray band in Figure 4, which consists of thirty-two terms.

## 6.0 A Study of Two Cloud Areas

NAA's were computed from the coefficients of FFT's of the 3 nm resolution satellite imagery for 20 October 1976. Two well separated areas, each of which contained a roughly homogeneous cloud field over at least a 200 nm square, were selected for the data sample. Identification of the clouds in these areas was made solely from the only available hard copy - a small, poor quality, transparency of a DMSP global mosaic. Area 1 was classified as a mixture of stratus (St) and stratocumulus (Sc) clouds and area 2 was classified as a uniform deck of St or fog. FFT's were performed on each 200 nm square area as well as on the 64 - 25 nm sq (8 x 8 pixels) boxes that made up the larger areas.

Figures 5 and 6 are the means of the NAA for 64 - 25 x 25 nm boxes as a function of frequency for area 1 and area 2 respectively. There are no great differences between the NAA's of the two areas, other than at frequency 0. The difference in frequency 0 indicates that the average brightness of area 1 is greater than area 2. Figures 7 and 8 are graphs of NAA for each 200 x 200 nm area respectively. Examination of Figures 7 and 8 supports what is seen in Figures 5 and 6.

A statistic was computed to determine whether the differences in mean NAA of the two areas as a function of frequency were significant using each 25 x 25 nm box. The statistic, T' measured  $\bar{u}_1 - \bar{u}_2$  for each frequency where  $\bar{u}_1$  represents the mean NAA's for area 1 and  $\bar{u}_2$  represents the mean NAA's for area 2. Table I lists the statistics T' as a function of frequency. At the 0.01 level of significance any T' larger than 2.576 or smaller than -2.576 indicates that an important difference in mean NAA exists. Table I shows that there is no significant difference in mean NAA for frequencies 1,

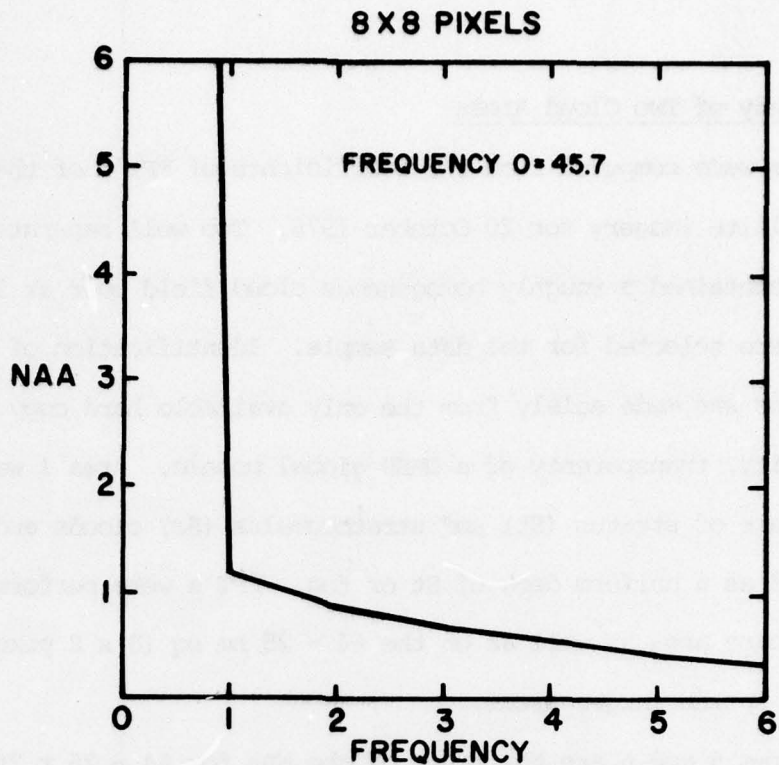


**FIG. 5 MEAN NORMALIZED AVERAGED AMPLITUDES (NAA) FOR 64 - 25 x 25 NM BOXES AS A FUNCTION OF FREQUENCY FOR AREA 1.**

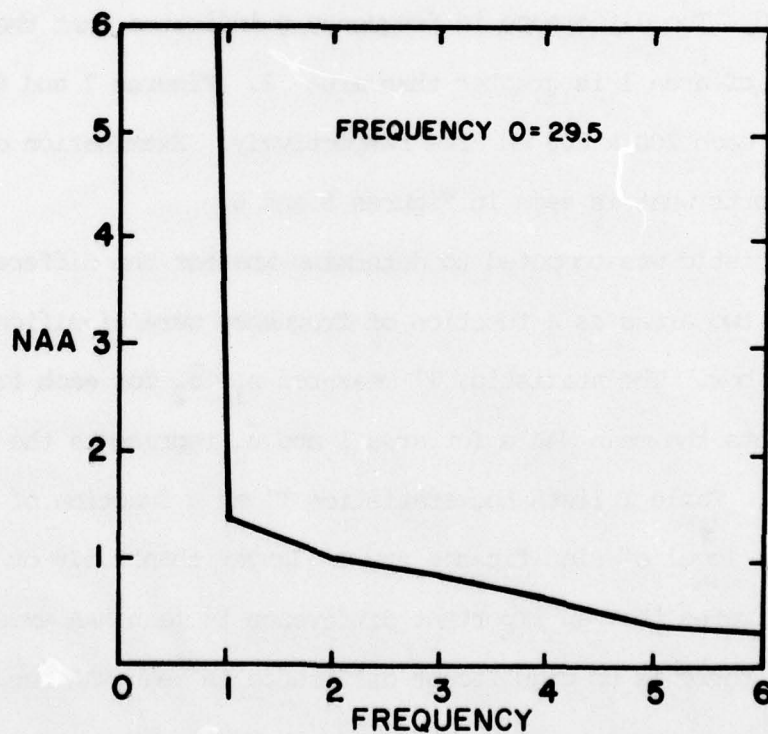


**FIG. 6 MEAN NORMALIZED AVERAGED AMPLITUDES (NAA) FOR 64 - 25 x 25 NM BOXES AS A FUNCTION OF FREQUENCY FOR AREA 2.**



64 X 64 PIXELS

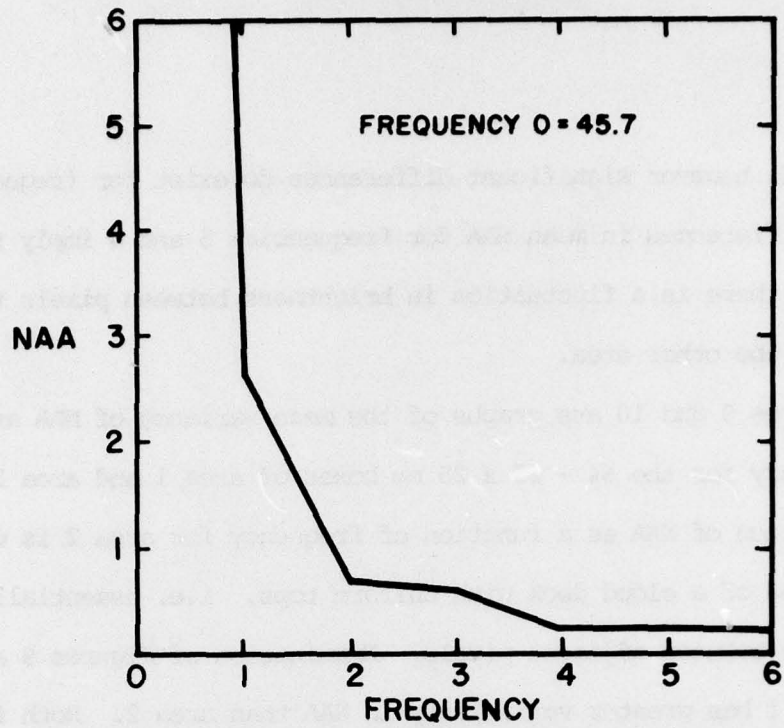


FIG. 7 NORMALIZED AVERAGED AMPLITUDES (NAA) FOR THE 200 x 200 NM BOX AS A FUNCTION OF FREQUENCY FOR AREA 1.

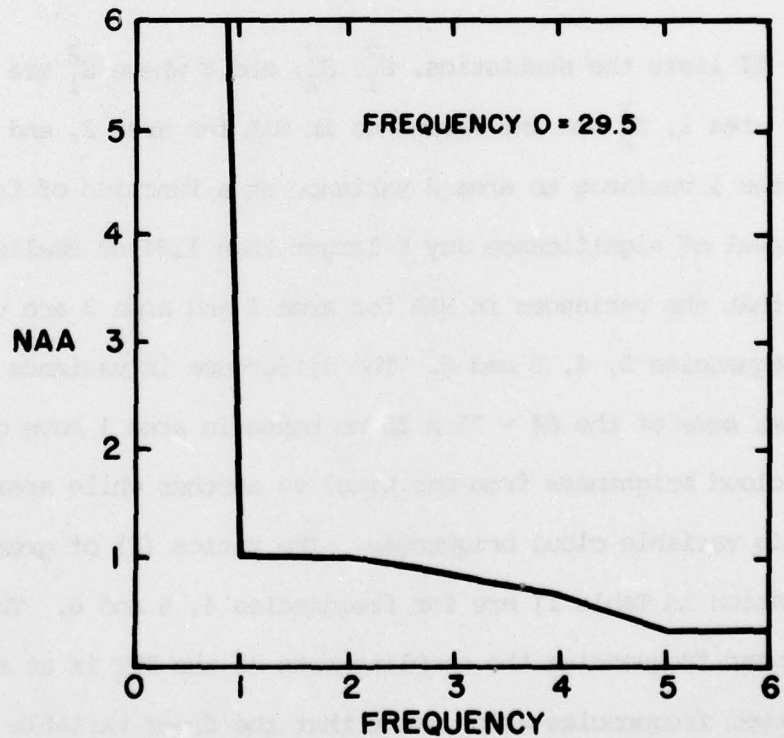
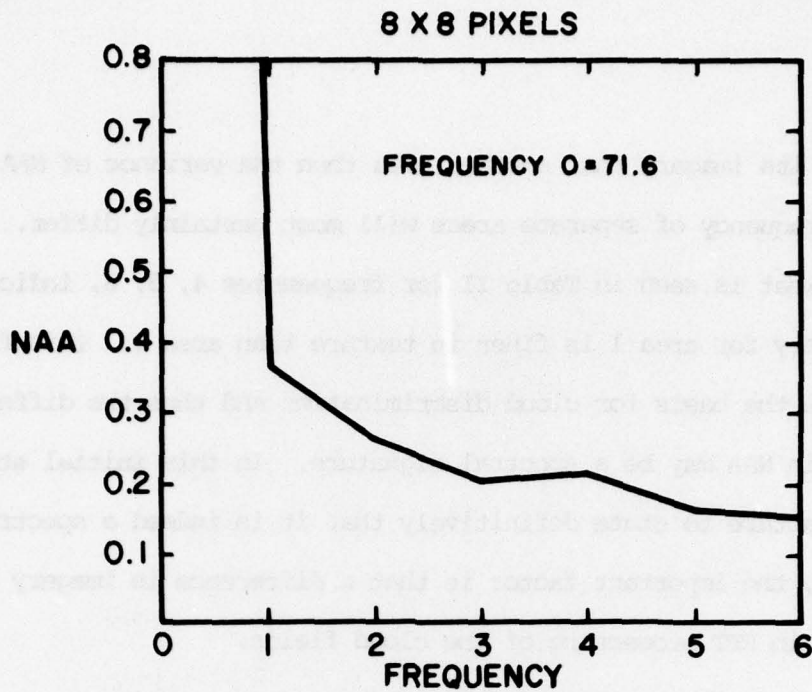


FIG. 8 NORMALIZED AVERAGED AMPLITUDES (NAA) FOR THE 200 x 200 NM BOX AS A FUNCTION OF FREQUENCY FOR AREA 2.

2, 5 and 6, however significant differences do exist for frequencies 0, 3 and 4. Differences in mean NAA for frequencies 3 and 4 imply that in one of the areas there is a fluctuation in brightness between pixels that does not appear in the other area.

Figures 9 and 10 are graphs of the mean variance of NAA as a function of frequency for the 64 - 25 x 25 nm boxes of area 1 and area 2 respectively. The variation of NAA as a function of frequency for area 2 is what would be expected of a cloud deck with uniform tops, i.e. essentially identical brightness between adjacent pixels. Examination of Figures 9 and 10 shows that area 1 has greater variability in NAA than area 2. Both figures show the same trend; however the variances are higher in area 1, indicating a cloud deck with non-uniform tops and/or breaks above satellite sensor resolution.

Table II lists the statistics,  $S_1^2$ ,  $S_2^2$ , and  $F$  where  $S_1^2$  are the variances in NAA for area 1,  $S_2^2$  are the variances in NAA for area 2, and  $F$  is the ratio of area 1 variance to area 2 variance as a function of frequency. At the 0.01 level of significance any  $F$  larger than 1.84 or smaller than 0.54 indicates that the variances in NAA for area 1 and area 2 are very different for frequencies 0, 4, 5 and 6. The difference in variance for frequency 0 means that some of the 64 - 25 x 25 nm boxes in area 1 have greater variability in cloud brightness from one pixel to another while area 2 does not exhibit this variable cloud brightness. The ratios ( $F$ ) of greatest interest and implication in Table II are for frequencies 4, 5 and 6. The reason is that at higher frequencies the sampling rate of the FFT is at a higher cycle than the lower frequencies which means that the finer variable brightness in the imagery is being sampled. Thus if one area has a finer variable



**FIG. 9 VARIANCE OF NORMALIZED AVERAGED AMPLITUDES (NAA) FOR 64-25 x 25 NM BOXES AS A FUNCTION OF FREQUENCY FOR AREA 1.**

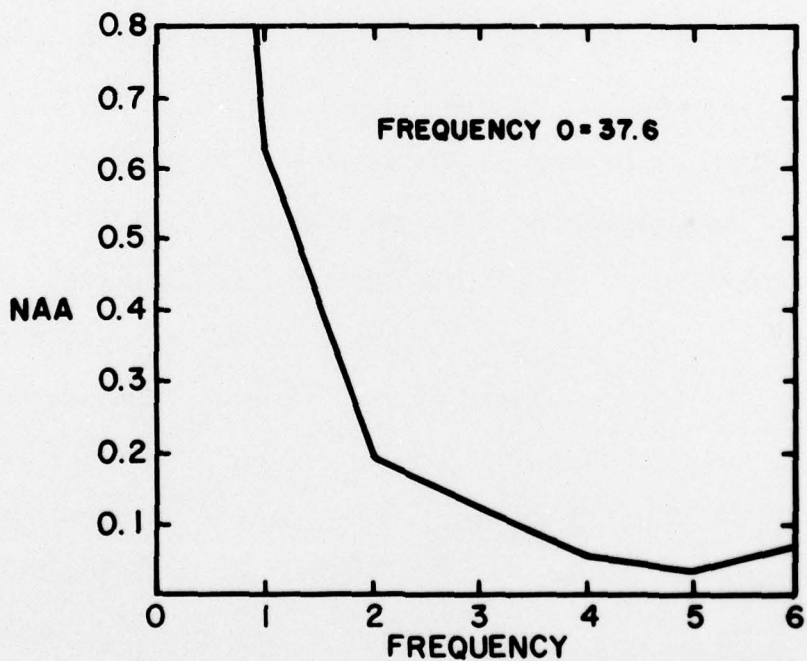


**FIG. 10 VARIANCE OF NORMALIZED AVERAGED AMPLITUDES (NAA) FOR 64-25 x 25 NM BOXES AS A FUNCTION OF FREQUENCY FOR AREA 2.**



brightness in its imagery than another area then the variance of NAA as a function of frequency of separate areas will most certainly differ. This is precisely what is seen in Table II for frequencies 4, 5, 6, indicating that the imagery for area 1 is finer in texture than area 2. This finer texture may be the basis for cloud discrimination and thus the differences in variances in NAA may be a spectral signature. In this initial study it would be conjecture to state definitively that it is indeed a spectral signature. However, the important factor is that a difference in imagery has been detected in FFT processing of the cloud fields.

## 7.0 Conclusions

This preliminary investigation of using second order statistics to identify cloud types from 1/3 nm resolution data was based on 3 nm resolution data for test purposes. Nevertheless, there is an indication that processing of Fast Fourier Transform coefficients, as described in Section 5.0, will allow classification of cloud types through a discriminant function. As in any spectral analysis, there is no substitute for adequate spectral and spatial resolution. For example, satellite data of 1/3 nm resolution would undoubtedly enhance the high frequency distinctions of spatial cloud distribution. This would give greater discriminating power among the class conditional covariances of the spectra. Then, using a diagonal covariance matrix, quadratic discriminants would classify the imagery field into its proper cloud category. This aspect of the investigation is now under way.

## 8.0 Future Work

This report is a preliminary study based on the earliest data available from AFGWC. Although 3 nm imagery was used, differences in the cloud fields were detected by processing FFT output. In the light of this, it is expected that FFT output from 1/3 nm imagery will yield sufficient differences between cloud types to allow automated classification using discriminant analysis. Questions of how many cloud types can be identified using discriminant analysis, their error bounds, and additional processing of FFT output (such as estimation of the class conditional covariance matrices of NAA) that will be required, must remain open until processing of 1/3 nm imagery is complete.

Plans for extending this work include using coincident Block 5-D DMSP visual and infrared imagery for FFT processing and cloud type classification through discriminant analysis. Improvements on cloud classification by meteorologists and looking at the nearest neighbor classification for persistence will be considered.



TABLE 1

<u>FREQUENCY</u>	<u>T' (d<sub>0</sub> = 0)</u>
0	12.3865
1	-1.3084
2	-1.6793
3	-3.2153
4	-2.2957
5	0.3690
6	-0.0855

The statistic  $T'$  for comparison of differences in means for area #1 and #2 (64 - 25 x 25 nm boxes). The null hypothesis is  $H_0: \bar{u}_1 - \bar{u}_2 = d_0$  and the alternative hypothesis is  $H_1: \bar{u}_1 - \bar{u}_2 \neq d_0$  where  $d_0 = 0$ . The symbols  $\bar{u}_1$  and  $\bar{u}_2$  are the mean normalized average amplitudes for area 1 and area 2 respectively. The critical region implying  $d_0 \neq 0$  is  ${}^t_{0.005} < T' < -{}^t_{0.005}$  for a type I error. Critical value for  ${}^t_{0.005}$  with 63 degrees of freedom is  ${}^t_{0.005} = 2.576$ .

TABLE 2

<u>Frequency</u>	<u><math>s_1^2</math></u>	<u><math>s_2^2</math></u>	<u><math>F=s_1^2/s_2^2</math></u>
0	71.599	37.583	1.9051
1	0.358	0.617	0.5802
2	0.262	0.186	1.4086
3	0.196	0.123	1.5953
4	0.213	0.053	4.0198
5	0.157	0.031	5.0645
6	0.150	0.069	2.1739

The statistic F in comparison of variance for area #1 and area #2 (64-25 x 25 nm boxes). The null hypothesis is  $H_0: \sigma_1^2 = \sigma_2^2$  and the alternative hypothesis is  $H_1: \sigma_1^2 \neq \sigma_2^2$ . For area 1 and area 2 respectively  $\sigma_1^2$  and  $\sigma_2^2$  are the variances in normalized amplitudes. The critical region implying  $\sigma_1^2 \neq \sigma_2^2$  is  $f\alpha/2 < f < 1/f\alpha/2$  for a type I error. Critical values for  $f_{0.005}$  and  $1/f_{0,005}$  are 1.84 and 0.54 respectively.